J Radioanal Nucl Chem (2013) 295:445–457
DOI 10.1007/s10967-012-1791-1

The worldwide NORM production and a fully automated gamma-ray spectrometer for their characterization

G. Xhixha · G. P. Bezzon · C. Broggini · G. P. Buso · A. Caciolli · I. Callegari · S. De Bianchi · G. Fiorentini · E. Guastaldi · M. Kaçeli Xhixha · F. Mantovani · G. Massa · R. Menegazzo · L. Mou · A. Pasquini · C. Rossi Alvarez · M. Shyti

Received: 1 April 2012 / Published online: 29 April 2012

Abstract Materials containing radionuclides of natural origin and being subject to regulation because of their radioactivity are known as Naturally Occurring Radioactive Material (NORM). By following International Atomic Energy Agency, we include in NORM those materials with an activity concentration, which is modified by human made processes. We present a brief review of the main categories of non-nuclear industries together with the levels of activity concentration in feed raw materials, products and waste, including mechanisms of radioisotope enrichments. The global management of NORM shows a high level of complexity, mainly due to different degrees of radioactivity enhancement and the huge amount of worldwide waste production. The future tendency of guidelines concerning environmental protection will require both a systematic monitoring based on the ever-increasing sampling and high performance of gamma-ray spectroscopy. On the ground of these requirements a new low-background fully automated high-resolution gamma-ray spectrometer MCA_Rad has been developed. The design of lead and cooper shielding allowed to reach a background reduction of two order of magnitude with respect to laboratory radioactivity. A severe lowering of manpower cost is obtained through a fully automation system, which enables up to 24 samples to be measured without any human attendance. Two coupled HPGe detectors increase the detection efficiency, performing accurate measurements on small sample volume (180 cm^3) with a reduction of sample transport cost of material. Details of the instrument calibration method are presented. MCA_Rad system can measure in less than one hour a typical NORM sample enriched in U and Th with some hundreds of Bq kg^{-1}, with an overall uncertainty less than 5 %. Quality control of this method has been tested. Measurements of three certified reference materials RGK-1, RGU-2 and RGTh-1 containing concentrations of potassium, uranium and thorium comparable to NORM have been performed. As a result, this test achieved an overall relative discrepancy of 5 % among central values within the reported uncertainty.

Keywords HPGe · Gamma-ray spectrometry · Industrial waste/by-product · NORM · Non-nuclear industry · Reference materials

G. Xhixha (✉) · S. De Bianchi · G. Fiorentini · F. Mantovani · M. Shyti
Dipartimento di Fisica, Università di Ferrara, Polo Scientifico e Tecnologico Via Saragat, 1, 44100 Ferrara, Italy
e-mail: xhixha@fe.infn.it

G. Xhixha · G. Fiorentini · F. Mantovani · M. Shyti
Ferrara Section, Istituto Nazionale di Fisica Nucleare (INFN), Via Saragat, 1, 44100 Ferrara, Italy

G. Xhixha
Faculty of Forestry Science, Agricultural University of Tirana, Kodër Kamëz, 1029 Tiranë, Albania

G. P. Bezzon · G. P. Buso · G. Fiorentini
Legnaro National Laboratory, Istituto Nazionale di Fisica Nucleare (INFN), Via dell'Università, 2, 35020 Legnaro, Padua, Italy

C. Broggini · A. Caciolli · R. Menegazzo · C. R. Alvarez
Padova Section, Istituto Nazionale di Fisica Nucleare (INFN), Via Marzolo 8, 35131 Padua, Italy

A. Caciolli · I. Callegari · E. Guastaldi · G. Massa · L. Mou · A. Pasquini
Center for GeoTechnologies, University of Siena, Via Vetri Vecchi, 34, 52027 San Giovanni Valdarno, Arezzo, Italy

M. Kaçeli Xhixha
Botanical, Ecological and Geological Sciences Department, University of Sassari, Piazza Università 21, 07100 Sassari, Italy

Introduction

Materials containing radionuclides of natural origin and being subject to regulation because of their radioactivity are known as NORM (Naturally Occurring Radioactive Material). By following IAEA, we include in NORM those materials with an activity concentration altered by human made processes[1] [37, 40]. In the last decades the large production of NORM and the potential long-term radiological hazards, due to long-lived radionuclides, represented an increasing level of concern. The development of instruments devoted to the measurements of NORM concentrations is a crucial task for the evaluation of the radiological impact on both workers and public members.

NORM are found as products, by-products and/or wastes of industrial activities, such as production of non-nuclear fuels (e.g. coal, oil and gas), mining and milling of metalliferous and nonmetalliferous ores (e.g. aluminum, iron, copper, gold and mineral sand), industrial minerals (e.g. phosphate and clays), radioisotope extraction and processing, as well as water treatments [38].

The most important sources of natural radioactivity are due to the presence of ^{238}U, ^{232}Th and ^{40}K in the Earth. Generally ^{235}U and ^{87}Rb and other trace elements are negligible. The decay chain of ^{238}U (^{232}Th) includes 8 (6) alpha decays and 6 (4) beta decays respectively, which are often associated with gamma transitions. The detection of these radioactivity sources can be performed through a wide set of methods, such as gamma-ray spectroscopy, alpha spectroscopy, neutron activation analysis (NAA), inductively-couple plasma mass-spectroscopy (ICP-MS), inductively coupled plasma atomic emission spectroscopy (ICP-AES), X-ray fluorescence spectroscopy (XRF) and liquid scintillation counting (LSC) [39]. The choice of the methodology for determining radioactive content of NORM depends on many factors, especially the economic character and prompt measurement of the individual samples.

Usually, in NORM ^{238}U and ^{232}Th decay chains are not in secular equilibrium. It means that in ^{238}U decay chain, some long-lived radionuclides (^{238}U, ^{226}Ra, ^{210}Pb) represent the head of decay chain segments, which can reach the secular equilibrium in less than one year: the gamma-ray spectrometry, therefore, is the suitable technique for measuring the abundance of these radionuclides and for checking the secular equilibrium among the respective chain segments. NORM can be enriched in ^{230}Th and ^{210}Po, which can be out of chain segments: the activities of ^{230}Th can be determined by gamma-spectrometry directly, while the suitable technique for quantifying ^{210}Po concentration is alpha spectrometry. In ^{232}Th decay chain the two chain segments, having on head ^{228}Ra and ^{228}Th, reach the secular equilibrium in about one month. By measuring the gamma transitions in each chain segment, one can determine ^{228}Ra and ^{228}Th abundances; while XRF, NAA, ICP-AES, ICP-MS are suitable techniques for measuring ^{232}Th content.

By using high-resolution gamma-ray spectrometry, all radioisotopes of ^{238}U and ^{232}Th decay chains, with the exception of ^{232}Th and ^{210}Po, can be investigated simultaneously. The radioactivity characterization of NORM may require a massive amount of measures of samples. For this purpose we designed and built up a low-background high-resolution gamma-ray spectrometry system, which allows an autonomous investigation of the radioactivity content on a large amount of samples, without any human attendance.

An empirical method for the characterization of the absolute efficiency of this instrument is presented in detail. Along with the instrument calibration, a quality test of this method was carried out. We tested the performances of the instrument by using three reference materials RGK-1, RGU-1 and RGTh-1 certified by IAEA and containing radioactive concentration comparable to NORM values.

Industrial processes producing NORM: an overview

Non-nuclear fuels extraction and processing

Oil and gas industry

Most hydrocarbons are trapped within porous reservoirs (known as oil/tar sand and oil shale deposits) by impermeable rocks above: the rock formations holding the oil also contain U and Th at the order of some ppm, corresponding to a total specific activity of some tens[2] of Bq kg^{-1}. Oil and gas reservoirs contain a natural water layer (formation water) that lies under the hydrocarbons: U and Th do not go into solution, but the formation water tends to reach a specific activity of the same order of the rock matrix [50] due to dissolution of ^{226}Ra and ^{228}Ra radium as radium chloride [33]. Additional heated water is often injected into the reservoirs to achieve maximum oil recovery. This process disturbs the cation/anion ratio and alters the solubility of various sulfate salts, particularly $BaSO_4$ and $RaSO_4$: radium co-precipitates with barium as sulfates forming scale within the oil pipes [41]. The solids,

[1] Sometimes these materials are known in the literature as TENORM (technologically enhanced naturally occurring radioactive material).

[2] The U and Th abundances vary for different rock types: e.g. in considering shale, the range of U and Th abundances reported by [17] are 2.4–3.4 and 8.5–14.3 ppm respectively. We remind that the specific activity of 1 ppm U (Th) corresponds to 12.35 (4.06) Bq/kg.

Table 1 Range of specific activity concentrations of ^{226}Ra and ^{228}Ra in scale and sludge, as reported by different authors for various geographic regions

Authors of the study	Country	^{226}Ra (10^4 Bq kg^{-1})		^{228}Ra (10^4 Bq kg^{-1})	
		Scale	Sludge	Scale	Sludge
Godoy and Cruz [31]	Brazil	1.91–32.3	0.036–36.7	0.421–23.5	0.025–34.3
Gazineu et al. [29]	Brazil	12.1–95.5	0.24–350	13.1–79.2	205
Gazineu and Hazin [28]	Brazil	7.79–211	0.81–41.3	10.2–155	0.94–11.8
Shawky et al. [70]	Egypt	0.754–14.3	0.0018	3.55–66.1	1.33
Abo-Elmaged et al. [1]	Egypt	49.3–51.9	0.527–0.886	3.20–5	0.1–0.19
Bakr [9]	Egypt	0.0016–0.0315	0.00055–0.179	0.00007–0.0177	0.00007–0.0885
Omar et al. [55]	Malaysia	0.055–43.4	0.0006–0.056	0.09–47.9	0.0004–0.052
Lysebo et al. [46]	Norway	0.03–3.23	0.03–3.35	0.01–0.47	0.01–0.46
Al-Saleh and Al-Harshan [6]	Saudi Arabia	0.00008–0.00015	0.00068–0.00594	0.000014–0.00031	0.00063–0.00476
Al-Masri and Suman [5]	Syria	14.7–105	47–100	4.3–18.1	35.9–66
Jonkers et al. [43]	USA	0.01–1500	0.005–80	0.005–280	0.05–50
Zielinski et al. [85]	USA	1.88–489	2.04–6.38	0.118–19	0.241–0.574

Remind that the exemption level recommended by [36] is 10^4 Bq kg^{-1} for both ^{226}Ra and ^{228}Ra

which are dissolved in crude oil and in the produced water, precipitate forming the sludge, which is a mixture of oil, carbonates and silicates sediments, as well as corrosion products that accumulate inside piping and in the bottom of storage tanks. The contribution to the radioactivity content in the sludge comes mainly from the precipitates of hard insoluble radium sulfate and possibly from radioactive silts and clays [33]. The specific activity of scales and sludges can vary enormously and generally it is of several orders of magnitude more than formation water. As reported in Table 1, the high variability, often among the samples collected in the same area, shows that a frequent and dense sampling of these NORM may be required.

Coal-fired power plant

Coal is a combustible sedimentary rock formed through the anaerobic process of the decomposed dead plants accumulated at the bottom of basins of some marsh land, lake or sea: the coalification process yields a product rich in carbon and hydrogen [65]. The organic matter plays an important role in the uranium concentrations at syngenetic, epigenetic and diagenetic stages of the sedimentary cycle [54]. The complexation and reduction of uranium are considered the main geochemical processes of the fixation of uranium on organic matter from very dilute solutions. The complexation of uranium involves the uranyl cation (UO_2^{2+}) producing a UO_2 complex through a dehydrogenation process of organic matter. During the reduction of the soluble UO_2^{2+}, the insoluble UO_2 is produced precipitating as uraninite [45]. The efficiency of these processes depends on the chemistry of the organic matter and on the temperature of reaction, producing U concentrations ranged over a couple orders of magnitude: the typical range of radionuclide activity concentrations of ^{238}U, ^{232}Th and ^{40}K in coal can be 10–600, 10–200 and 30–100 Bq kg^{-}1 respectively [10]. The geological processes over the time increase the grade of coal transforming the organic material from peat to graphite. In low-grade coal the secular equilibrium between ^{238}U and ^{232}Th and their decay products is not expected while in the high-grade coal it may exist [74]. The volatilization–condensation process of particles during coal combustion breaks the secular equilibrium and increases the radionuclide concentrations with decreasing of particle size: the maximum enrichment has been measured in particles with diameters of about 1 μm. ^{210}Pb and ^{210}Po exhibit the greatest enrichment, as much as a factor of 5, while maximum enrichment for uranium isotopes is about a factor of 2, and for ^{226}Ra a factor of around 1.5. In some samples of fly ash the ^{210}Pb and ^{226}Ra activity exceeds thousands of Bq kg^{-1} [27].

According to the World Coal Institute [84] 40 % of the world's electricity in 2003 is generated by coal: in the same year the world coal consumption reached 48.4×10^{11} kg [80]. After the combustion of the bituminous coal containing an average ash of 12 %, coal by-products are composed by some 70 % of fly ash and by some 30 % of the bottom ash and boiler slag. A large fraction (more than 95 %) of these small particles can be removed from gas stream, by usually applying electrostatic precipitator and fabric filters: in 2003 the estimated worldwide fly ash production was 3.9×10^{11} kg [53]. In 2003 the US and EU fly ash production was about 0.6×10^{11} kg and 0.4×10^{11} kg respectively. In US and UE about 39 and 48 % of this amount was recycled respectively [2, 25]. According to [80] the world coal consumption in 2035 is

projected to reach 93.8×10^{11} kg, corresponding to an estimated fly ash production of 7.5×10^{11} kg. This large amount of NORM is required to be measured and monitored with accuracy, by developing fast and ad hoc methods: the MCA_Rad system presented in "MCA_Rad system" section has been designed as a response to this increasing demand.

Metal mineral extraction and processing

Bauxite extraction and alumina production

In metal mining and waste processing, the radioactive content varies from 10^{-2} kBq kg^{-1}, for the large volume industry, to 10^{2} kBq kg^{-1} for rare earth metals [38]. In massive metal extraction, the amount of NORM produced by bauxite processing is relevant.

Bauxites generally contain concentrations of Th and U greater than the Earth's crustal average: in a multi-methodological study published by Adams and Richardson [3] based on 29 samples of bauxites from different locations, the reported specific activities of U and Th are in the range 33–330 and 20–532 Bq kg^{-1} respectively. These values can be compared with the typical concentration in bauxite: 400–600 Bq kg^{-1} for U and 300–400 Bq kg^{-1} for Th [79].

The parent rocks affect the U and Th abundances in the bauxites: in particular the bauxites derived from acid igneous rocks show a concentration higher than those extracted from basic igneous rocks, whereas the bauxites mined from deposits of shales and carbonates rocks are characterized by intermediate concentrations. The process of lateritization during bauxite formation contributes to increase the ratio Th/U, which is generally more than 4 [3].

Bayer process is used for refining bauxite to smelting grade alumina, the aluminum precursor: it involves the digestion of crushed bauxite in a concentrated sodium hydroxide solution at temperatures up to 270 °C. Under these conditions, the majority of the species containing aluminum is dissolved in solution in the ore, while the insoluble residues are filtered making a solid waste called "red mud". The alumina is obtained by the hydroxide solution after the processes of precipitation and calcination [34]. Finally, by using the Hall–Heroult electrolytic process, alumina is reduced to aluminum metal.

The fact that thorium and radium in a hydroxide medium are practically insoluble [73] could disturb especially the secular equilibrium of the uranium chain, as it has been observed in some measurements [62]. However, some "results indicate that the chemical processing of the bauxite ore has not significant consequences in the secular equilibrium of either the uranium or thorium series" [18]. In the process of extracting alumina from bauxite, over 70 % of the thorium and radium are concentrated in the red mud [3].

Table 2 Activity concentration in red mud reported in the literature (a) the range indicated correspond to the maximum and minimum value measured for different samples and in (b) the uncertainties of measurement results. The activities quoted are assumed equal to ^{228}Ac in (1), equal to ^{228}Th in (2) and equal to ^{238}U in (3)

Authors of the study	Country	Activities (Bq kg^{-1})	
		^{226}Ra	^{232}Th
Papatheodorou et al. [56][(a)]	Greece	13–185	15–412
Philipsborn and Kuhnast [60][(b),(1)]	Germany	122 ± 18	183 ± 33
Pinnock [61][(a)]	Jamaica	370–1047	328–350
Somlai et al. [73][(a)]	Hungary	225–568	219–392
Akinci and Artir [4][(b)]	Turkey	210 ± 6	539 ± 18
Jobbágy et al. [42][(a)]	Hungary	102–700	87–545
Cooper et al. [18][(b),(2)]	Australia	310 ± 20	1350 ± 40
Turhan et al. [78][(a)]	Turkey	128–285	342–357
Pontikes et al. [62][(b),(2)]	Greece	379 ± 43	472 ± 23
Beretka and Mathew [12]	Australia	326	1129
Georgescu et al. [30]	Romania	212	248
Döring et al. [23][(b)]	Germany	190 ± 30	380 ± 50
Ruyters et al. [66][(3)]	Belgium	550	640

In 2009 the worldwide production of bauxite and alumina was 199×10^9 and 123×10^9 kg respectively. Considering that the worldwide ratio bauxite/alumina, averaged in the period 1968–2009, is 2.7 ± 0.1, we expect that 1.7 ± 0.1 kg of red mud is generated per kg of alumina [83]. By assuming that at least 70 % of the radioisotopes in bauxite accumulate in the red mud, the increasing factor of radioactivity content in the red mud varies in a range of 1.1–1.6. Using these estimated enrichments for bauxite we encompass a large portion of the radium and thorium activities of the red mud reported in literature (Table 2).

Based on recent statistics, more than 70×10^9 kg of red mud is discharged annually in the world: it constitutes the most important disposal problem of the aluminum industry. The mud is highly basic (pH > 10) and its storage on huge area can cause environmental pollution, soil basification, paludification, surface water and groundwater pollution as well as resource pollution. The safe treatment of this NORM is an increasing social problem. Moreover, a considerable attention has been given to additional uses of bauxite wastes: they include metallurgical extractions, building materials productions and the development of new ceramics and catalytic materials. Gamma-ray spectrometers are able to process thousands of measurements in order to perform environmental monitoring and to control the

recycled by-products. The MCA_Rad system described in "MCA_Rad system" section could be extremely helpful for processing these measurements by significantly diminishing manpower costs.

Mineral sand and downstream productions

The extraction of mineral sand ore is important for the production of heavy minerals (with densities heavier than 2.8 g cm^{-3}) like titanium, tin and zirconium bearing minerals and rare earth elements[3] (REEs) The deposits of hard minerals, which do not undergo erosion and transport processes, mainly occur when they have been concentrated by marine, alluvial and/or wind processes. These placer deposits can be found also in vein deposits, mostly disseminated in alkaline intrusions in hard rocks. The radioactivity concentration of mineral sand can be of the order of a few hundreds Bq kg^{-1}, depending on the placer geology. In heavy minerals we can often find high content of radioactivity, sometimes of the order of hundreds kBq kg^{-1}.

The process involved in heavy mineral extraction includes two main phases of separation. The first phase separates the heavy mineral concentration, by using either dry operation or dredging of the slurried ore: this produces high amount of residues with a radionuclide concentration of the same order of mineral sand [59]. During the second phase, the heavy mineral concentration is further separated mainly by combining dry magnetic and electrostatic processes. This allows the concentration of various minerals, such as titanium bearing minerals (ilmenite, leucoxene, rutile), zircon bearing minerals (zircon, baddeleyite) and REEs bearing minerals (monaxite, zenotime). The products of this second phase generally show a high content of radioisotopes.

Titanium bearing minerals are used mainly to produce TiO_2 pigment. The radioactivity concentration in these minerals varies in rutile (400–2900 Bq kg^{-1} Th and 250–500 Bq kg^{-1} U) and ilmenite (400–4100 Bq kg^{-1} Th and 250–750 Bq kg^{-1} U) [38, 48, 76]. The higher production efficiency is obtained by rutile: it is directly processed through the chloride route producing TiO_2 pigment/waste with a ratio of 5/1 [81]. Since the radioisotopes follow the liquid waste stream, the radioactivity concentration in the waste is very high due to the severe mass reduction.

[3] REEs contain 16 chemical elements, including those with atomic numbers 57 (lanthanum) through 71 (lutetium), as well as yttrium (atomic number 39), which has similar chemical properties.

Ilmenite requires a pre-processing in order to produce synthetic rutile: the product/waste ratio is 10/7. The synthetic rutile is further processed through the chloride route in order to produce TiO_2 pigment with a product/waste ratio of 5/6, showing a light enhancement of radioactivity concentration in waste of ilmenite processing [38].

In TiO_2 pigment production the most relevant NORM are made by the chloride treatment of rutile. The worldwide production of TiO_2 in 2010 was about 5.7×10^9 kg when the mineral extraction ratio is 1/10 for rutile/ilmenite [38, 82]: about 2 % of the total waste which has been generated can show a strong enhancement in radioactivity concentration.

The most common zirconium bearing minerals are zircon and baddeleyite: in 2010 the world extraction of these minerals was about 1.2×10^9 kg [82]. Mineral sands containing zircon are commonly used in ceramic and refractory industries. The zircon crystal lattice host uranium and thorium: their activities in zircon bearing minerals are in the range of 1–5 kBq kg^{-1} for U and of 0.5–1 kBq kg^{-1} for Th respectively [64].

The manufacture of zirconia is mainly performed by fusion of feedstock with coke near to zirconium molten temperatures. It causes the dissociation of mineral in ZrO_2 and SiO_2: during the fusion U and Th end up almost at the same concentration in zircon product, while ^{226}Ra tends to end up in silica, causing the disequilibrium of U decay chain. The subsequent caustic fusion process at 600 °C increases the purity of zirconia. During the chemical dissolution, zircon crystal structure is destroyed, yielding nearly 100 % of uranium recovery in the form of sodium uranate [14]. The performances of MCA_Rad system completely fit the need of measuring radioactivity content in this kind of NORM.

The main minerals used as sources of REEs can be extracted by placer deposits (monazite and xenotime) and by hard rocks (bastnaesite, coperite and pyrochlore). Monazite minerals are characterized by high activity concentration of U (25–75 kBq kg^{-1}) and Th (41–575 kBq kg^{-1}). The chemical attack of the mineral based on NaOH separates sodium phosphate from a mixture called "cake I", which is rich in heavy minerals. Cake I is further filtered, given that it yields a concentration of rare earth chlorides and a mixture called "cake II" containing most of thorium and uranium originally present in monazite feedstock [58]. The decay chain of U and Th are not in secular equilibrium in cake II: thorium precipitates while radium remains in solution. The latter can reach very high activities (7 and 10 MBq kg^{-1} for ^{226}Ra and ^{228}Ra respectively) [59]. In 2010, the extraction of monazite has been 1.3×10^8 kg [82] and its processing has made 10 % of cake II waste [57]. This large amount of highly enhanced radioactivity NORM requires scrupulous monitoring and control.

Industrial minerals extraction and processing

Phosphate fertilizer industry

The main phosphate-rock (phosphorite) deposits are both of igneous and sedimentary origin and they are part of the apatite group. They are commonly encountered as fluor-apatite and francolite respectively. A specific characteristic of phosphate rocks consists in a low ratio Th/U, in general <0.5, which is mainly due to relative high concentrations of uranium commonly between 370 and 2470 Bq kg^{-1} and sometimes higher than 12.35 kBq kg^{-1}. Uranium and thorium decay chains are generally found to be in secular equilibrium [49].

Phosphorite is mainly processed through the so-called "wet process", which includes chemical treatments, mostly by using sulfuric acid: the products are phosphoric acid (PA) and an insoluble calcium sulfate salt called phosphogypsum (PG), with a ratio PG/PA = 5 [75]. PA and PG are usually separated by filtration and reactor off-gas and vapors. These processes concentrate the trace elements in PA or PG in various amounts causing secular disequilibrium in U and Th decay chains. In PG is found approximately 80–90 % of the ^{226}Ra along with a high content of ^{210}Pb and ^{210}Po [11, 15], as a consequence of the similar chemistry [11, 32]. About 80–85 % of the uranium [11, 63] and about 70 % of thorium [75] concentrate in PA. As a consequence of these processes, we expect a relevant enhancement of U concentration in PA and an abundance of Ra in PG comparable with that in phosphate-ore (Table 3). The high production of posphogypsum requires constant controls in order to make a secure stockage and reutilization of such material. These controls must be extended to PA and phosphate fertilizers: the MCA_Rad system described in the next section has been designed to deal with automatic gamma-ray measurements on large amounts of PA and PG samples.

MCA_Rad system

An accurate radiological characterization of NORM requires careful investigation on a case-by-case basis. Indeed the NORM issue shows high levels of complexity mainly due to the huge amount of worldwide waste production perturbed by the different geochemical composition of raw materials and the effective concentration of a wide range of industrial processes. Most of current studies show that determining the content of ^{226}Ra, ^{228}Ra and ^{40}K radioisotopes in NORM is mandatory for radiation protection. High-resolution gamma-ray spectrometry is a frequently used non-destructive technique, which provides an accurate identification and quantitative determination of such radioisotopes.

A strategic approach to the NORM issue consists in constructing systematic monitoring programs. However, this approach is often limited by funding and manpower capacities of a laboratory. Indeed, when a laboratory deals with random measurements, the main costs are determined by the instrument investment program; instead, for a routine monitoring program the substantial costs are due to the manpower involved. The MCA_Rad system introduces an innovative configuration of a laboratory high-resolution gamma-ray spectrometer featured with a complete automation measurement process. Two HPGe detectors allow to achieve both good statistical accuracy in a short time and ad hoc approach to low-background shielding construction design. This self-constructed instrument drastically minimizes measurement and manpower costs.

Set-up design and automation

The core of the MCA_Rad system is made of two 60 % relative efficiency coaxial p-type HPGe gamma-ray detectors, which possess an energy resolution of about 1.9 keV at 1332.5 keV (^{60}Co). Both detectors are controlled by individual integrated gamma spectrometers for

Table 3 Studies on activities of phosphate rock (PR) and phosphogypsum (PG) in different countries

Authors of the study	Country	^{238}U (Bq kg^{-1})		^{226}Ra (Bq kg^{-1})	
		PR	PG	PR	PG
Mazilli et al. [47]	Brazil			130–1445	93–729
Silva et al. [71]	Brazil	434–1128	66–140	407–1121	228–702
Saueia et al. [69]	Brazil	14–638	<2–61	53–723	24–700
Santos et al. [67]	Brazil	102–1642	32–69	239–862	307–1251
Saueia et al. [68]	Brazil	158–1868	40–58	139–1518	122–940
EM Afifi et al. [26]	Egypt	916	140	890	459
Azouazi et al. [8]	Morocco	2100–2450	–	1850–2320	1420
Carvalho [15]	Portugal	1003	26–156	1406	950–1043
Hull and Burnett [35]	USA (Central Florida)	848–1980	45–368	882–1980	505–1353
	USA (Northern Florida)	242–982	23–452	230–883	270–598

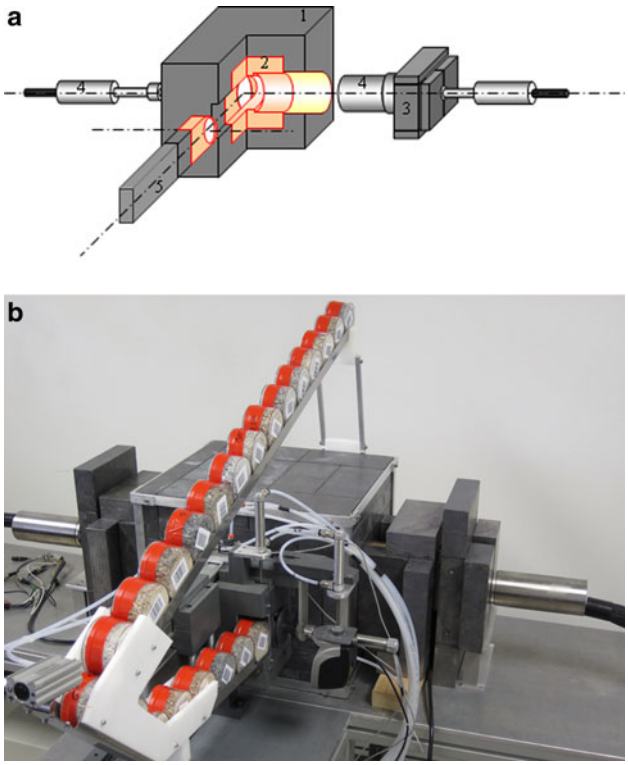

Fig. 1 **a** Schematic design of the MCA_Rad system. (1) The main lead shielding construction (20 cm × 25 cm × 20 cm). (2) The core copper shielding (10 cm × 15 cm × 10 cm). (3) Rear lead shielding construction. (4) HPGe semiconductor detectors. (5) The mechanical sample changer. **b** View of the MCA_Rad system

the digital signal processing. The new cooling technology, which employs mechanical coolers, allows to simplify the management of the system. The detectors are accurately shielded and positioned facing each other 5 cm apart (Fig. 1a).

The background spectrum of a gamma-ray spectrometer is mainly due to the combination of cosmic radiation, environmental gamma radiation and the radioactivity produced by radio-impurities both in the shielding materials and in the detector. In order to effectively reduce the environmental gamma radiation, an adequate shielding construction is needed.

In the MCA_Rad a 10 cm thick lead house shields the detector assembly, leaving an inner volume around the detectors of about 10 dm^3 (Fig. 1a, b). The lead used as shielding material adds some extra background due to the presence of ^{210}Pb, produced by ^{238}U decay chain. This isotope, which has an half life of 22.3 years, is revealed by a gamma energy of 46.5 keV and a *bremsstrahlung continuum* from beta decay of its daughter ^{210}Bi extending from low energy up to 1162 keV. Furthermore, when a gamma-ray strikes the lead surface, characteristic lead X-rays may escape and hit the detector [72].

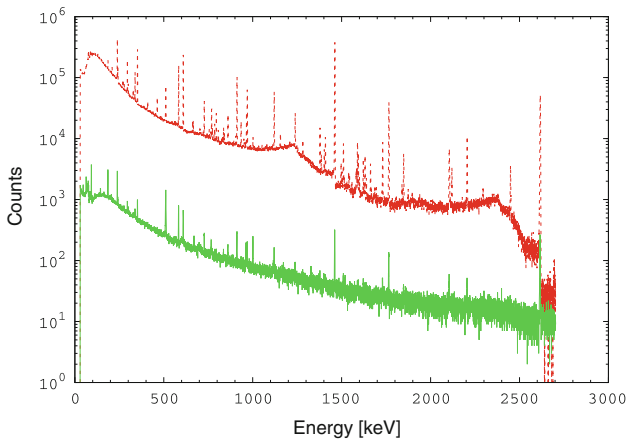

Fig. 2 The MCA_Rad system background spectra (acquisition live time 100 h) with (*continuous line*) and without (*dashed line*) shielding. Spectra are obtained by summing the single detector background after rebinning with 0.33 keV/channel

The inner volume is occupied by 10 cm thick oxygen free copper house, which allows to host the sample under investigation. In order to reduce the X-rays coming from the sample, the end-cup windows of the detectors is further shielded with a tungsten alloy sheet of 0.6 mm. A 10 mm thick bronze cylinders and walls of about 10 cm of lead are also shielding the rear part of the system (Fig. 1a, b). The final intrinsic background is reduced by two order of magnitude compared to other unshielded detectors (see Fig. 2).

As a good practice of gamma-ray spectrometry analysis, information concerning background spectra is required both to detect any potential residual contaminations and for background corrections. A background measurement with acquisition time of several days is performed regularly. The final sensitivity of the measurements can be evaluated by using the detection limit (L_D) described in [19], assuming the Gaussian probability distribution of the number of counts in the background (B) and rejecting the data not included in a range of 1.645σ (95 % confidence level):

$$L_D = 2.71 + 4.65\sqrt{B} \simeq 4.65\sqrt{B} \quad (1)$$

where the approximation is admitted for high number of counts. The minimum detectable activity (MDA) for the background is calculated using the L_D, according to the formula:

$$\mathrm{MDA} = \frac{L_D}{\varepsilon I_\gamma t} \quad (2)$$

where ε is the absolute efficiency (calculated as described below), I_γ is the gamma line intensity and t is the acquisition live time. In Table 4 we report the typical one hour acquisition live time background counts and the sensitivity of the measurement expressed by L_D and MDA for the

Table 4 MCA_Rad system characterization of typical one hour (live time) background (B in counts) for the most important energies and the corresponding detection limit L_D and minimum detectable activity (MDA) [19] for 95 % confidence interval (CI)

Parent isotope	Daughter isotope	Energy (keV)	B (counts)	L_D (counts)	MDA (Bq)
^{238}U	^{234m}Pa	1001.0	8 ± 1	21	22.16
	^{214}Pb	351.9	31 ± 2	49	0.50
	^{214}Bi	609.3	44 ± 1	32	0.49
^{232}Th	^{228}Ac	911.2	27 ± 1	27	0.94
	^{212}Pb	238.6	100 ± 2	62	0.46
	^{212}Bi	727.3	10 ± 1	31	3.00
	^{208}Tl	583.2	42 ± 1	33	0.71
^{40}K	^{40}K	1460.8	151 ± 1	19	5.53

main gamma lines used to calculate the radionuclide concentrations in NORM.

The sample material is contained in a cylindrical polycarbonate box of 75 mm in diameter, 45 mm in height and 180 cm^3 of useful volume, labeled by a barcode. Up to 24 samples can be charged in a slider moving by gravity and further introduced at the inner chamber through an automatic "arm" made of copper, lead and plastic closing the lateral hole of the housing (Fig. 1b). The mechanical automation consists on a barcode scanner and a set of compressed air driven pistons. This mechanism not only makes the sample identification possible, but is also able to introduce/expel the samples. All operations, including measurements, are controlled by a PC by means of a dedicated software.

The program receives by the operator an input file with relevant information about the slot of samples: acquisition live time, spectra file name, sample weight, sample description and barcode. The procedure is repeated until the barcode reader detects samples. A new batch command file is generated to be successively employed in spectrum analysis. In order to complete the automation of the MCA_Rad system, a user-friendly software has been developed for spectra analysis. The code adopts ANSI No. 42 [7] standard specification for the peak analysis.

Calibration and data analysis

For each measurement, the final spectrum is obtained by adding, after rebinning, the two simultaneously measured spectra: for this purpose an accurate energetic calibration of the system, along with a periodical check, is required. When a shift larger than 0.5 keV is observed, the energy calibration procedure is repeated.

The absolute photopeak efficiency (ε_P) for the MCA_Rad system has been determined by using standard point sources method, and producing the calibration curve. Two low activity point sources with complex decay schemes are used [22]: a certified ^{152}Eu source, with an activity of 6.56 kBq in 1995, known with an uncertainty of 1.5 % and a ^{56}Co home made source, that has been normalized relative to ^{152}Eu by calculating the activity of the 846.8 keV (^{56}Co) gamma line. The ^{56}Co source is used in order to extend the efficiency calibration for gamma energies up to 3,000 keV.

The spectra obtained are corrected for: (1) coincidence summing, C_{CS}, on each individual detector, produced by the complex decay scheme of the sources, (2) differences between the geometry of the point sources and the sample shape, C_G and (3) self-attenuation, C_A, of gamma-rays within the sample volume.

The correction due to coincidence summing is studied by following the method described in [21] and obtained as a relationship between the single total efficiency (ε_t), the single apparent absolute photopeak efficiency (ε_p^{app}) and isotope decay data. The single total efficiency is obtained by estimating the peak-to-total ratio (P/T) using the empirical approach described by [16] and recalling the relationship $\varepsilon_p^{app}/\varepsilon_t = P/T$. The decay coefficients for ^{152}Eu were calculated from decay data taken from [52], while those for ^{56}Co were taken from [24, 77]. Finally, the absolute efficiency, $\varepsilon_p(E)$, of the MCA_Rad system is given by the sum of single HPGe detector contribution corresponding to the characteristic gamma energies (E_i) of the standard calibration sources used.

$$\varepsilon_p(E_i) = \varepsilon_p^{app}(E_i) C_{CS}(E_i) \quad (3)$$

Then the absolute efficiency is obtained for the energetic range from 200 to 3,000 keV by fitting them using the function given by [44] (Fig. 3):

$$\varepsilon\,(\%) = (b_0 E/E_0)^{b_1} + b_2 \exp(-b_3 E/E_0) + b_4 \exp(-b_5 E/E_0) \quad (4)$$

where E (keV) is the gamma-ray energy; $E_0 = 1$ keV is introduced to make dimensionless the argument of the exponential dimensionless and b_i are the fitting parameters (where $b_0 = 1.38$, $b_1 = 1.41$, $b_2 = 22.97$, $b_3 = 5.43$, $b_4 = 6.61$ and $b_5 = 0.44$).

The effect of volume geometry can be described in terms of the effective solid angle developed analytically by [51] within less than 2 % of uncertainty between numerical

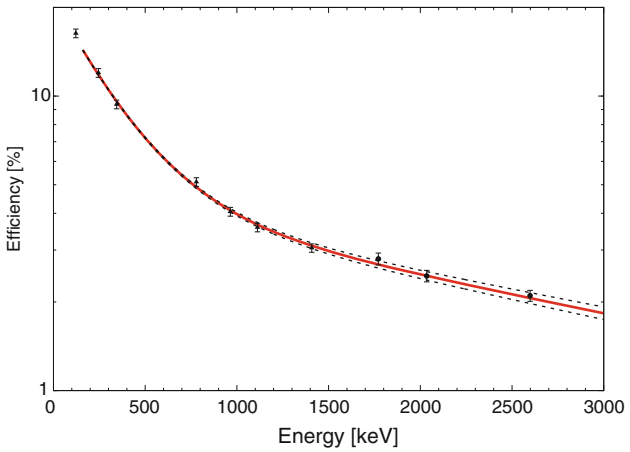

Fig. 3 Absolute efficiency curve of MCA_Rad system. It is obtained by fitting ^{152}Eu (*triangle*) and ^{56}Co (*circle*) energies with Eq. 2 performing the best fit. *Dashed curves* represent ± one sigma uncertainty interval

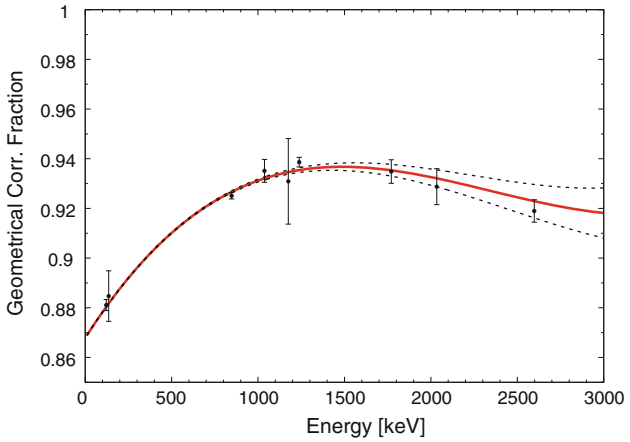

Fig. 4 The geometrical correction factor due to differences between calibration (point source) and measurement geometry (cylinder of 75 mm of diameter and 45 mm of height), which is obtained by fitting nine photopeaks of ^{56}Co and ^{57}Co with a third order polynomial. *Dashed curves* represent ± one sigma uncertainty interval

and experimental calculations. The geometrical factor (Fig. 4) for MCA_Rad system is deduced from a set of measurements using a ^{56}Co and ^{57}Co point sources placed at different radial distances (center, middle and lateral) from the detector axis at different planes, reconstructing the sample geometry using the formula:

$$C_{\mathrm{G}}(E_i) = \frac{\bar{\Omega}_x}{\bar{\Omega}_{ref}} \approx \frac{1}{R_{ref}(E_i)} \sum_{j=1}^{N} \frac{[R_x(E_i)]_j}{N} \tag{5}$$

where $R_x(E_i)$ is the net count rate in the standard spectrum collected in different positions (j) and $R_{ref}(E_i)$ is the net count rate in the standard spectrum collected in the reference positions (center). The geometrical correction factor is obtained as a function of energy by fitting a third order polynomial as a function of energy (Fig. 4):

$$C_{\mathrm{G}}(E) = \sum_{i=0}^{4} a_i \left(\frac{E}{E_0}\right)^i \tag{6}$$

where $E_0 = 1$ keV is introduced to make the argument dimensionless and a_i are the fitting coefficients ($a_0 = 0.8678$, $a_1 = 0.1098$, $a_2 = -0.0541$, $a_3 = 0.0077$).

The gamma-ray attenuation correction C_{SA} is calculated for different kind of samples taking into account their differences in density by a simplified expression deduced by [13, 20]:

$$C_{\mathrm{SA}} = \frac{1 - \exp(-\mu_l t)}{\mu_l t} \tag{7}$$

where $\mu_l = \mu\rho$ (cm^{-1}) is the linear mass attenuation coefficient, μ (cm^2 g^{-1}) is the mass attenuation coefficient, ρ (g cm^{-3}) is the sample density and t (cm) is the sample effective thickness (which in our case is the half thickness of the sample container). The mass attenuation coefficient is strongly Z dependent in the energy range below few hundred keV while for higher energies the trend is smoother and it depends mainly on energy. These features can be used, since NORM characterization, especially concerning ^{226}Ra, ^{228}Ra and ^{40}K, requires the investigation of gamma-rays with energies higher than hundreds keV. We can parameterize the mass attenuation coefficient as a function of energy. We used XCOM 3.1 database, which is available on-line and developed by the Nuclear Institute of Standards and Technology (NIST). It is calculated by using for various rocks forming minerals, the average mass attenuation coefficient was deduced with a standard deviation of less than 2 % in the energetic range 200–3,000 keV.

$$\bar{\mu}(E) = \sum_{i=0}^{2} a_i [\ln(E)]^i \tag{8}$$

where a_i ($a_0 = 0.5593$, $a_1 = -0.1128$, $a_2 = 0.0590$) are coefficients determined by fitting this function with a reduced χ^2 of $\chi^2_v = 1.12$. Finally the self-attenuation correction factor was given as a function of gamma-ray energy and sample density through the relationship:

$$C_{\mathrm{SA}}(E, \rho_{\mathrm{s}}) = \exp\left[b_0 + b_1 \ln(E) + b_2 \ln(E)^2\right] \rho_s \tag{9}$$

Table 5 Uncertainty budged for absolute efficiency determination

Uncertainty source	Relative uncertainty (%)
Certified standard source uncertainty	1.5[a]
Coincidence summing correction factor	<2
Geometrical correction factor	<2
Self-attenuation correction factor	<2

[a] 95 % of confidence level

Table 6 In the sixth column we report the activity concentrations (in Bq kg^{-1}) calculated for the main energetic lines used for ^{238}U and ^{232}Th decay chains and for ^{40}K together with respective statistical uncertainties

Parent isotope	Daughter isotope	E (keV)	C^*_{CS}	C_{SA}	Activity (Bq kg^{-1})	Certified reference material activity (Bq kg^{-1})
^{238}U	^{234m}Pa	1001.0	1.000	1.24	4875 ± 48	4940 ± 30
	^{214}Bi	609.3	1.190	1.32	4872 ± 4	
	^{214}Pb	351.9	1.002	1.42	4773 ± 3	
^{232}Th	^{228}Ac	911.2	1.024	1.24	3092 ± 4	3250 ± 90
	^{212}Pb	238.6	0.990	1.48	3246 ± 2	
	^{212}Bi	727.3	1.056	1.27	3389 ± 9	
	^{208}Tl	583.2	1.298	1.31	3342 ± 4	
^{40}K		1460.8		1.21	14274 ± 71	14000 ± 400

The reference material activities certificated by IAEA are shown in seventh column. The correction coefficients C^*_{CS} and C_{SA} are referred to coincidence summing and self-absorption respectively

where b_i ($b_0 = 1.2609$, $b_1 = -0.2547$, $b_2 = 0.0134$) are coefficients determined by fitting this function.

The uncertainty budged for the calibration procedure is reported in Table 5. Considering the uncertainties due to geometrical and self-attenuation correction factors as systematic errors, the overall uncertainty about the absolute efficiency of the MCA_Rad system is estimated to be <5 %.

Measurement of reference materials

The applicability of the MCA_Rad system as well as the method quality control was cross checked using certified reference materials containing concentrations comparable to NORM values. Three reference materials certified within 95 % of confidence level prepared in powder matrix (240 mesh) containing ^{238}U (IAEA RGU-1) 4,940 ± 30 Bq kg^{-1}, ^{232}Th (IAEA RGTh-1) 3,250 ± 90 Bq kg^{-1} in secular equilibrium and ^{40}K (IAEA RGK-1) 14,000 ± 400 Bq kg^{-1} are used. The sample boxes were filled with the reference materials, after were dried at 60 °C temperature, hermetically sealed and then left undisturbed for at least 3 weeks in order to establish radioactive equilibrium in ^{226}Ra decay chain segment prior to be measured.

In Table 6 we report the specific activity calculated for the principal gamma lines used to estimate the isotopes of uranium and thorium decay chain and for potassium using the formula:

$$A\ (\mathrm{Bq/kg}) = \frac{R}{\varepsilon I_\gamma m} C_{SA} C_G C^*_{CS} \quad (10)$$

where R is the measured count rate (background corrected), ε is the absolute efficiency, I_γ is the gamma line intensity, m is the mass of the sample, C_{SA} is the correction factors for self-absorption, C_G is the geometrical correction factor and C^*_{CS} is the coincidence summing correction factor (calculated using the same approach as described above for the specific decay chains of the uranium and thorium). The results have an overall relative discrepancy of less than 5 % among certified central values within the reported uncertainty.

Conclusions

We presented a summary of the main categories of non-nuclear industries together with the levels of activity concentration in feeding raw materials, products, by-products/waste and the possible enhancement mechanisms. The main chemical and physical processes that disturb the secular equilibrium of uranium and thorium decay chains have been reported. The degree of radioactivity enhancement is studied along with the radioactivity level in feeding raw material and the industrial process involved. A refined estimation of radioactivity concentrations of ^{226}Ra, ^{228}Ra and ^{40}K in NORM is almost impossible in such a wide range of industrial activities: the strategy that we propose consist in a systematic monitoring and continuous checking based on high-resolution gamma-ray spectroscopy.

For this purpose an innovative approach to the configuration of a laboratory low-background high-resolution gamma-ray spectrometer, MCA_Rad system, was developed and featured with fully automated measurement processes. It presents the following advantages.

- The new design of lead and cooper shielding configuration allowed to reach a background reduction of two order of magnitude respect to laboratory radioactivity.
- A severe lowering of manpower cost is obtained by a fully automation system which permits to measure up to 24 samples without any human attendance.
- The two HPGe detectors offer higher detection efficiency: confronting the MDA of the system with typical

NORM values, it can be deduced that measurements in less than one hour are realized with uncertainties of less than 5 %.

- Accurate measurements are performed on small sample volume (180 cm^3) with a reduction of material transport costs.
- A user-friendly software has been developed in order to analyze a high number of spectra, possibly with automatic procedure and customized output.

An empirical efficiency calibration method using multi-gamma standard point sources is discussed. The correction factors affecting the measured spectra (coincidence summing, sample shape, sample gamma-ray self-attenuation) are given with respective procedures. As a result of this procedure the absolute efficiency is estimated to have an overall uncertainty of less than 5 %. A test of the applicability of the instrument as well as the method quality control using certified reference materials showed an overall relative discrepancy of less than 5 % among certified central values within the reported uncertainty.

We, therefore, conclude that the MCA_Rad system shows efficacy in the face of the NORM issue, by increasing the capacities of a laboratory and offering accurate results with a reduction of manpower costs.

Acknowledgments We are grateful for useful comments and discussions to P. Altair, M. Baldoncini, E. Bellotti, L. Carmignani, L. Casini, V. Chubakov, T. Colonna, M. Gambaccini, Y. Huan, W. F. McDonough, G. Oggiano, R. L. Rudnick and R. Vannucci.This work was partially supported by INFN (Italy) and by Fondazione Cassa di Risparmio di Padova e Rovigo.

References

1. Abo-Elmagd M, Soliman HA, Salman KhA, El-Masry NM (2010) Radiological hazards of TENORM in the wasted petroleum pipes. J Environ Radioact 101:51–54
2. ACAA (American Coal Ash Association) (2003) 'Fly Ash facts for highway engineers'. Federal Highway Association Report FHWA-IF-03-019
3. Adams JAS, Richardson KA (1960) Thorium, uranium and zirconium concentration in bauxite. Econ Geol 55:1653–1675
4. Akinci A, Artir R (2008) Characterization of trace elements and radionuclides and their risk assessment in red mud. Mater Charact 59:417–421
5. Al-Masri MS, Suman H (2003) NORM waste management in the oil and gas industry: The Syrian experience. J Radioanal Nucl Chem 256:159–162
6. Al-Saleh FS, Al-Harshan GA (2008) Measurements of radiation level in petroleum products and wastes in Riyadh City Refinery. J Environ Radioact 99:1026–1031
7. ANSI No. 42.14 (1999) American national standard for calibration and use of germanium spectrometers for the measurement of gamma-ray emission rates of radionuclides
8. Azouazi M, Ouahidi Y, Fakhi S, Andres Y, Abbe JCh, Benmansour M (2001) Natural radioactivity in phosphates, phosphogypsum and natural waters in Morocco. J Environ Radioact 54:231–242
9. Bakr WF (2010) Assessment of the radiological impact of oil refining industry. J Environ Radioact 101:237–243
10. Beck HL (1989) Radiation exposures due to fossil fuel combustion. Int J Radiat Appl Instrum, Part C. Radiat Phys Chem 34:285–293
11. Beddow H, Black S, Read D (2006) Naturally occurring radioactive material (NORM) from a former phosphoric acid processing plant. J Environ Radioact 86:289–312
12. Beretka J, Mathew PJ (1983) Natural Radioactivity of Australian building material wastes and by-products. Health Phys 48:87–95
13. Bolivar JP, Garcia-Leon M, Garcia-Tenorio R (1997) On self-attenuation corrections in gamma-ray spectrometry. Appl Radiat Isot 48:1125–1126
14. Brown AEP, Costa EC (1972) Processing of a uraniferous zirconium ore. IEA Publication N. 274
15. Carvalho FP (1995) ^{210}Pb and ^{210}Po in sediments and suspended matter in the Tagus estuary, Portugal. Local enhancement of natural levels by wastes from phosphate ore processing industry. Sci Total Environ 159:201–214
16. Cesana A, Terrani M (1989) An empirical method for peak-to-total ratio computation of a gamma-ray detector. Nuclear Instrum Methods Phys Res A 281:172–175
17. Condie KC (1993) Chemical composition and evolution of the upper continental crust: Contrasting results from surface samples and shales. Chem Geol 104:1–37
18. Cooper MB, Clarke PC, Robertson W, Mcpharlin IR, Jeffrey RC (1995) An investigation of radionuclide uptake into food crops grown in soils treated with Bauxite mining residues. J Radioanal Nucl Chem 194:379–387
19. Currie LA (1986) Limits for Qualitative Detection and Quantitative Determination Application to Radiochemistry. Anal Chem 40:586–593
20. Cutshall NH, Larsen IL, Olsen CR (1983) Direct analysis of Pb-210 in sediment samples: self-absorption corrections. Nuclear Instrum Methods 206:309–312
21. De Felice P, Angelini P, Fazio A, Biagini R (2000) Fast procedures for coincidence-summing correction in gamma-ray spectrometry. Appl Radiat Isot 52:745–752
22. DeFelice P, Fazio A, Vidmar T, Korun M (2006) Close-geometry efficiency calibration of p-type HPGe detectors with a Cs-134 point source. Appl Radiat Isot 64:1303–1306
23. Döring J Beck T, Beyermann M, Gerler J, Henze G, Mielcarek J, Schkade (2007) Exposure and radiation protection for work areas with enhanced natural radioactivity NORM V (Proc. Conf. Seville, Spain 2007)
24. Dryák P, Kovář P (2009) Table for true summation effect in gamma-ray spectrometry. J Radioanal Nucl Chem 279:385–394
25. ECOBA (European Coal Combustion Products Association) (2003) CCP Production & Use Survey-EU 15
26. El Afifi EM, Hilal MA, Attallah MF, EL-Reefy SA (2009) Characterization of phosphogypsum wastes associated with phosphoric acid and fertilizers production. J Environ Radioact 100:407–412
27. Flues M, Camargo IMC, Silva PSC, Mazzilli BP (2006) Radioactivity of coal and ashes from Figueira coal power plant in Brazil. J Radioanal Nucl Chem 270:597–602
28. Gazineu MHP, Hazin CA (2008) Radium and potassium-40 in solid wastes from the oil industry. Appl Radiat Isot 66:90–94
29. Gazineu MHP, Araújo AA, Brandão YB, Hazin CA, Godoy JM (2005) Radioactivity concentration in liquid and solid phases of scale and sludge generated in the petroleum industry. J Environ Radioact 81:47–54
30. Georgescu D, Aurelian F, Popescu M, Radulescu C (2004) Sources of TENORM–Inventory of phosphate fertilizer and aluminum industry, NORM IV (Proc. Conf. Szczyrk

31. Godoy JM, Cruz RP (2003) ^{226}Ra and ^{228}Ra in scale and sludge samples and their correlation with the chemical composition. J Environ Radioact 70:199–206
32. Guimond RJ, Hardin JM (1989) Radioactivity released from phosphate-containing fertilizers and from gypsum. Radiat Physics Chem 34:309–315
33. Heaton B, Lambley J (1995) TENORM in the oil, gas and mineral mining industry. Appl Radiat Isot 46:577–581
34. Hind AR, Bhargava SK, Grocott SC (1999) The surface chemistry of Bayer process solids: a review. Coll Surf A:Physicochemical Engineering aspects 146:359–374
35. Hull CD, Burnett WC (1996) Radiochemistry of Florida phosphogypsum. J Environ Radioact 32:213–238
36. IAEA (International Atomic Energy Agency) (1996) International basic safety standards for protection against ionizing radiation and for the safety radiation sources. safety series no. 115. IAEA, Vienna
37. IAEA (International Atomic Energy Agency) (2003) Radioactive waste management glossary. IAEA, Vienna
38. IAEA (International Atomic Energy Agency) (2003) Extent of environmental contamination by naturally occurring radioactive material (NORM) and technological options for mitigation. technical reports series no. 419. IAEA, Vienna
39. IAEA (International Atomic Energy Agency) (2006) Assessing the need for radiation protection measures in work involving minerals and raw materials. safety reports series no. 49. IAEA, Vienna
40. IAEA (International Atomic Energy Agency) (2008) Naturally occurring radioactive material (NORM V), proceedings series. IAEA, Vienna
41. Jerez Vegueria SF, Godoy JM, Miekeley N (2002) Environmental impact studies of barium and radium discharges by produced waters from the "Bacia de Campos" oil-field offshore platforms, Brazil. J Environ Radioact 62:29–38
42. Jobbágy V, Somlai J, Kovács J, Szeiler G, Kovács T (2009) Dependence of radon emanation of red mud bauxite processing wastes on heat treatment. J Hazard Mater 172:1258–1263
43. Jonkers G, Hartog FA, Knaepen AAI, Lancee PFJ (1997) Characterization of NORM in the oil and gas production (E&P) industry, Radiological problems with natural radioactivity in the non-nuclear industry In: Proc. Int. Symp., Amsterdam
44. Knoll GF (1999) Radiation detection and measurements, 3rd edn. Wiley, New York
45. Landais P (1996) Organic geochemistry of sedimentary uranium ore deposits. Ore Geol Rev 11:33–51
46. Lysebo I, Birovljev A, Strand T (1996) NORM in oil production–occupational doses and environmental aspects.In: Proceedings of the 11th Congress of the Nordic Radiation Protection Society, Reykjavik, Iceland
47. Mazzilli B, Palmiro V, Saueia C, Nisti MB (2000) Radiochemical characterization of Brazilian phosphogypsum. J Environ Radioact 49:113–122
48. McNulty GS (2007) Production of titanium dioxide. In: Proc. Conf. Seville, Spain
49. Menzel RG (1968) Uranium, radium, and thorium content in phosphate-rocks and their possible radiation hazard. J Agric Food Chem 16:231–234
50. Metz V, Kienzler B, Schüßler W (2003) Geochemical evaluation of different groundwater–host rock systems for radioactive waste disposal. J Contam Hydrol 61:265–279
51. Moens L, De Donder J, Xi-lei L, De Corte F, De Wespelaere A, Simonits A, Hoste J (1981) Calculation of the absolute peak efficiency of gamma-ray detectors for different counting geometries. Nuclear Instrum Methods 187:451–472
52. Monographie BIPM-5 (2004) Table of Radionuclides, vol 2. Bureau International des Poids et Measure. ISBN 92-822-2207-1
53. Mukherjee AB, Zevenhoven R, Bhattacharya P, Sajwan KS, Kikuchi R (2008) Mercury flow via coal and coal utilization by-products: a global perspective. Resour Conserv Recycl 52:571–591
54. Nakashima S (1992) Complexation and reduction of uranium by lignite. The Sci Total Environ 117(118):425–437
55. Omar M, Ali HM, Abu MP, Kontol KM, Ahmad Z, Ahmad SHSS, Sulaiman I, Hamzah R (2004) Distribution of radium in oil and gas industry wastes from Malaysia. Appl Radiat Isot 60:779–782
56. Papatheodorou G, Papaefthymiou H, Maratou A, Ferentinos G (2005) Natural radionuclides in bauxitic tailings (red-mud) in the Gulf of Corinth, Greece. Radioprotection 1(40):549–555
57. Paschoa AS (1993) Overview of environmental and waste management aspects of the monazite cycle. Radiat Prot Australia 11:170–173
58. Paschoa AS (1997) Potential Environmental and Regulatory Implications of Naturally Occurring Radioactive Materials (NORM). Appl Radiat lsotopes 49:189–196
59. Paschoa AS (2008) NORM from the Monazite cycle and from the oil and gas industry: problems and tentative solutions. International conference on radioaecology and environmental radioactivity. In: Proc. Conf. Bergen, Norway
60. Philipsborn HV, Kuhnast E (1992) Gamma spectrometric characterization of industrially used African and Australian bauxites and their red mud tailings. Radiat Prot Dosimetry 45:741–744
61. Pinnock W (1991) Measurements of radioactivity in Jamaican building materials and gamma dose equivalents in a prototype red mud house. Health Phys 61:647–651
62. Pontikes Y, Vangelatos I, Boufounos D, Fafoutis D, Angelopoulos GN (2006) Environmental aspects on the use of Bayer's process bauxite residue in the production of ceramics. Adv Sci Technol 45:2176–2181
63. Poole AJ, Allington DJ, Baxter AJ, Young AK (1995) The natural radioactivity of phosphate ore and associated waste products discharged into the eastern Irish Sea from a phosphoric acid production plant. Sci Total Environ 173(174):137–149
64. Righi S, Andretta M, Bruzzi L (2005) Assessment of the radiological impacts of a zircon sand processing plant. J Environ Radioact 82:237–250
65. Rubio Montero MP, Durán Valle CJ, Jurado VargasM, Botet JiménezA (2009) Radioactive content of charcoal. Appl Radiat Isot 67:953–956
66. Ruyters S, Mertens J, Vassilieva E, Dehandschutter B, Poffijn A, Smolders E (2011) The red mud accident in Ajka (Hungary): plant toxicity and trace metal bioavailability in red mud contaminated soil. Environ Sci Technol 45:1616–1622
67. Santos AJG, Mazzilli BP, Fávaro DIT, Silva PSC (2006) Partitioning of radionuclides and trace elements in phosphogypsum and its source materials based on sequential extraction methods. J Environ Radioact 87:52–61
68. Saueia CHR, Mazzilli BP (2006) Distribution of natural radionuclides in the production and use of phosphate fertilizers in Brazil. J Environ Radioact 89:229–239
69. Saueia CH, Mazzilli BP, Fávaro DIT (2005) Natural radioactivity in phosphate rock, phosphogypsum and phosphate fertilizers in Brazil. J Radioanal Nucl Chem 264:445–448
70. Shawky S, Amer H, Nada AA, El-Maksoud TMA, Ibrahiem NM (2001) Characteristics of NORM in the oil industry from eastern and western deserts of Egypt. Appl Radiat Isot 55:135–139
71. Silva NC, Fernandes EAN, Cipriani M, Taddei MHT (2001) The natural radioactivity of Brazilian phosphogypsum. J Radioanal Nucl Chem 249:251–255
72. Smith ML, Bignell L, Alexiev D, Mo L, Harriso J (2008) Evaluation of lead shielding for a gamma-spectroscopy system. Nuclear Instrum Methods Phys Res A 589:275–279

73. Somlai J, Jobbàgy V, Kovàcs J, Tarjàn S, Kovàcs T (2008) Radiological aspects of the usability of red mud as building material additive. J Hazard Mater 150:541–545
74. Tadmor J (1986) Radioactivity from coal-fired power plants: a review. J Environ Radioact 4:177–204
75. Tayibi H, Choura M, López FA, Alguacil FJ, López-Delgado A (2009) Environmental impact and management of phosphogypsum. J Environ Manage 90:2377–2386
76. Timmermans CWM, van der Steen J (1996) Environmental and occupational impacts of natural radioactivity from some non-nuclear industries in The Netherlands. J Environm Radioact 32:97–104
77. Tomarchio E, Rizzo S (2011) Coincidence-summing correction equations in gamma-ray spectrometry with p-type HPGe detectors. Radiat Phys Chem 80:318–323
78. Turhan S, Arikan IH, Demirel H, Güngör N (2011) Radiometric analysis of raw materials and end products in the Turkish ceramics industry. Radiat Phys Chem 80:620–625
79. UNSCEAR (2000) (United Nations Scientific Committee on the Effects of Atomic radiation) Sources and effects of ionizing radiation. Report to the General Assembly of the United Nations with Scientific Annexes, United Nations Sales Publication E.00.IX.3, New York
80. US EIA/IOE (2010) US Energy Information Administration/ International Energy Outlook
81. USGS MCS (1996) US Geological Survey Mineral Commodities Summary
82. USGS MCS (2011) US Geological Survey Mineral Commodities Summary
83. USGS US Geological Survey Data Series 140, Kelly T, Buckingham D, DiFrancesco C, Porter K, Goonan T, Sznopek J, Berry C, Crane M (2002) Historical statistics for mineral commodities in the United States. US Geological Survey open-file report 01-006, minerals.usgs.gov/minerals/pubs/of-01-006/
84. WCI World Coal Institute (2005) Coal facts 2005 edition
85. Zielinski RA, Otton JK, Budahn JR (2001) Use of radium isotopes to determine the age and origin of radioactive barite at oilfield production sites. Environ Pollut 113:299–309